

Received January 20, 2022, accepted February 2, 2022, date of publication February 22, 2022, date of current version March 4, 2022.

Digital Object Identifier 10.1109/ACCESS.2022.3153703

# Generalized Approximate Message Passing Detector for GSM-OTFS Systems

TIEBIN WANG<sup>1</sup>, SHIWEN FAN<sup>2</sup>, HAO CHEN<sup>2</sup>, YUE XIAO<sup>2</sup>, (Member, IEEE),  
XUEMEI GUAN<sup>3</sup>, AND WENLONG SONG<sup>3</sup>

<sup>1</sup>Information and Computer Engineering College, Northeast Forestry University, Harbin 150006, China

<sup>2</sup>National Key Laboratory of Science and Technology on Communications, University of Electronic Science and Technology of China, Chengdu 611731, China

<sup>3</sup>College of Mechanical and Electrical Engineering, Northeast Forestry University, Harbin 150006, China

Corresponding author: Yue Xiao (xiaoyue@uestc.edu.cn)

This work was supported by the National Key Research and Development Program of China under Grant 2020YFB1807203.

**ABSTRACT** Orthogonal Time Frequency Space (OTFS) as a two-dimensional modulation scheme designed in the delay-Doppler domain, is realized by inverse symplectic finite Fourier transform (ISFFT) and symplectic finite Fourier transform (SFFT), for combating the high Doppler channels toward future wireless communications. Meanwhile, generalized spatial modulation (GSM) offers an efficient implementation for multi-input multi-output (MIMO) systems, by activating only part of the transmit antennas to alleviate inter-channel interference (ICI). In this paper, the combination of the above two concepts is exploited, for bridging their unique advantages. On the other hand, an iterative detector based on generalized approximate message passing (GAMP) is also developed for GSM-OTFS. Simulation results demonstrate that the proposed GAMP detector can achieve better performance than the conventional minimum mean square error (MMSE) detector.

**INDEX TERMS** Generalized spatial modulation, orthogonal time frequency space, generalized approximate message passing.

## I. INTRODUCTION


Toward the next generation wireless communication networks, it is up to devise a waveform with high robustness to time or frequency dispersions, for the sake of satisfying the demand of high-speed communication scenarios, like the high-speed train that speeds up to 300 km/h or even 500 km/h [1]. In such extreme data transmission scenarios with high Doppler shift, traditional orthogonal frequency division multiplexing (OFDM) [2], [3], which is a dominant modulation technique in the fourth generation (4G), suffers from significantly degraded performance.

Several schemes have been proposed for reducing the effect of the high Doppler shift [4]–[10]. One of the representative transmission techniques is orthogonal time frequency space (OTFS) [5]–[10], which promises block error rate performance improvements particularly in systems with high Doppler shift. With the aid of the inverse symplectic finite Fourier transform (ISFFT) and symplectic finite Fourier transform (SFFT), OTFS is capable of extracting the full diversity of both the time and frequency domains, and trans-

ferring the time varying multipath channel into an almost non-fading two-dimensional (2D) channel [6]. The results indicate that OTFS outperforms OFDM in the context of the high Doppler spreads scenario, which makes it an attractive design alternative.

More recently, the multiple-input multiple-output (MIMO) structures have been combined with OTFS for further spectral efficiency improvement [11]–[14], which reaps the time, space and frequency diversity. More specifically, the OTFS scheme provides full time and frequency diversity through the mapping in the delay-Doppler domain at the transmitter and the inverse process at the receiver, while the extra space diversity is obtained by the transmit and receive antennas in MIMO. However, the introduction of MIMO structure may impose additional interference, for example, inaccurate inter-antenna synchronization (IAS) and inter-channel interference (ICI), as well as the inter-antenna interference (IAI) at the receiver.

For the sake of avoiding the IAI and mitigating the ICI, a special regime, called spatial modulation (SM), has been integrated with OTFS [15]. Unlike MIMO-OTFS, each sub-carrier in SM-OTFS is only activated in one selected antenna for data transmission at each signaling time, while the index

The associate editor coordinating the review of this manuscript and approving it for publication was Md. Arafatur Rahman .

of the selected antenna also carries the bit information, which exploits the extra spatial degree of freedom. However, compared to that of the MIMO-OTFS scheme, the spectral efficiency of SM-OTFS decreases, especially when the number of transmit antenna is large.

One of the variants of SM termed generalized spatial modulation (GSM) [16]–[19], has the potential to solve this challenge, striking a good balance between spectral efficiency and bit error rate (BER) performance. Different from traditional SM, GSM activated several antennas instead of one antenna, achieving a moderate spectral efficiency and reduced IAI. Moreover, the effectiveness of the combination of GSM and traditional OFDM has been confirmed in the literature [20]. However, to the best of authors' knowledge, GSM has not been applied to OTFS and its performance has not yet to be studied. Against this background, the main contributions of the paper are summarized as follows.

- 1) We combine the idea of GSM and OTFS to reap their advantages, for the sake of achieving performance improvement in the high-speed communication scenarios, compared to that of MIMO-OTFS.
- 2) Moreover, the zero-forcing (ZF) criterion and the minimum mean square error (MMSE) criterion of the proposed GSM-OTFS scheme have been derived, in the context of the time dispersive channel and the doubly dispersive channel, respectively.
- 3) For further improving the equalized performance, an iterative detector based on the generalized approximate message passing (GAMP) criterion [21]–[23] has been proposed for the GSM-OTFS system, due to its low implementation complexity and excellent performance. Specifically, the proposed GAMP detector includes three types of nodes, namely, the received symbol, the transmitted symbol and the reconstructed non-interference symbol. Messages are iteratively exchanged among the above three types of nodes.
- 4) Finally, we analyze the computational complexity of the proposed GAMP detector, and simulate the system performance of conventional MIMO-OTFS and GSM-OFDM, on the condition that a high Doppler shift exists. The comparison of the BER performance discloses the advantage of the proposed GSM-OTFS system. And the simulation results also indicate the effectiveness of the proposed GAMP detector, compared to that of conventional MMSE detector.

The remainder of this paper is organized as follows. In Section II, a general description of the conventional MIMO-OTFS and GSM-OFDM have been provided, then the system model of our proposed GSM-OTFS is described, followed by the derivation of the ZF and MMSE criterion in the time dispersive channel and the doubly dispersive channel, respectively. Section III describes the proposed GAMP detector. In Section IV, we analyze the complexity of the proposed GAMP detector, while in Section V, we provide the

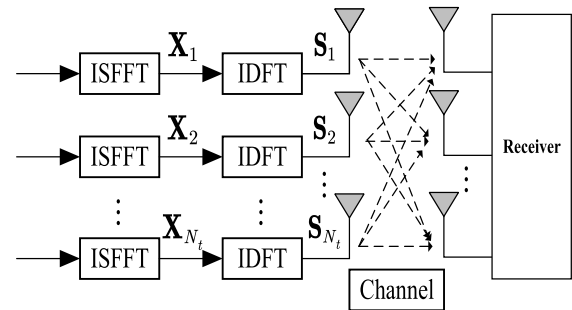


FIGURE 1. The block diagram of the MIMO-OTFS systems.

numerical and simulation results. Section VI concludes the paper.

*Notation:* Lower- and upper-case letters denote scalars, while Boldface lower- and upper-case letters denote vectors and matrices, respectively.  $(\cdot)^T$  and  $(\cdot)^H$  stand for the transpose and Hermitian transpose of a vector/matrix, respectively. Moreover, let  $\mathbf{a}(i)$  and  $\mathbf{A}(i, j)$  denote the  $i$ -th element of a vector  $\mathbf{a}$  and the  $(i, j)$ -th element of a matrix  $\mathbf{A}$ . We further let  $\mathbf{A} = \text{circ}[a_0, a_1, \dots, a_{N-1}] \in \mathbb{C}^{N \times N}$  denote the circulant matrix with the first column as  $\{a_0, a_1, \dots, a_{N-1}\}$ , and let  $\mathbf{A} = \text{diag}[a_0, a_1, \dots, a_{N-1}] \in \mathbb{C}^{N \times N}$  denote the diagonal matrix with  $\{a_0, a_1, \dots, a_{N-1}\}$  as diagonal elements. Furthermore,  $\mathbf{I}_n$  represents the  $n \times n$  identity matrix. And  $E\{\cdot\}$ ,  $\text{Var}\{\cdot\}$  and  $\text{trace}\{\cdot\}$  denote the expectation, variance and trace operation, respectively. What's more,  $[a]$  represents the largest integer less than  $a$ , and  $C_a^b$  represents the number of the combinations that selects  $b$  elements from a set with  $a$  different elements. Finally, we let  $\mathbf{F}_n$  and  $\mathbf{F}_n^H$  denote the  $n$ -point discrete Fourier transform (DFT) and inverse discrete Fourier transform (IDFT) matrices, where  $\mathbf{F}_n \mathbf{F}_n^H = \mathbf{I}_n$ .

## II. SYSTEM MODEL

In this section, in order to explain our proposed GSM-OTFS system more clearly, we first introduce the system model of MIMO-OTFS and GSM-OFDM, followed by the proposed GSM-OTFS.

### A. MIMO-OTFS

As shown in Fig. 1, multiple-input multiple-output (MIMO) techniques have been introduced to OTFS for achieving higher spectral and energy efficiency in the context of high-Doppler fading channels [11]–[14]. Specifically, we assume that the MIMO-OTFS system is equipped with  $N_t$  transmit antennas and  $N_r$  receive antennas, and each antenna independently transmits the OFDM-based OTFS modulated symbols. For the  $i$ -th antenna, the source bits are firstly mapped into a set of data symbols  $\{d_i(m, n); m = 1, 2, \dots, M; n = 1, 2, \dots, N\}$  in the context of the Doppler-delay domain, where  $M$  and  $N$  represent the number of subcarriers and slots respectively. Then, the data symbols are converted into the time-frequency domain by the inverse symplectic finite Fourier transform (ISFFT), which

can be expressed as

$$X_i(k, l) = \frac{1}{\sqrt{MN}} \sum_{m,n} d_i(m, n) e^{j2\pi \left( \frac{(n-1)(k-1)}{N} - \frac{(m-1)(l-1)}{M} \right)}, \quad (1)$$

where  $k = 1, 2, \dots, M, l = 1, 2, \dots, N$ . Hence, the time-frequency domain symbols can be obtained as

$$\mathbf{X}_i = \begin{bmatrix} X_i(1, 1) & X_i(1, 2) & \dots & X_i(1, N) \\ X_i(2, 1) & X_i(2, 2) & \dots & \vdots \\ \vdots & \vdots & \vdots & \vdots \\ X_i(M, 1) & X_i(M, 2) & \dots & X_i(M, N) \end{bmatrix}, \quad (2)$$

where  $i = 1, 2, \dots, N_t$ . Then the transmitted signal  $\mathbf{S}_i$  of the  $i$ -th transmit antenna is obtained by the inverse discrete Fourier transform (IDFT) operation as follows

$$\mathbf{S}_i = \begin{bmatrix} S_i(1, 1) & S_i(1, 2) & \dots & S_i(1, N) \\ S_i(2, 1) & S_i(2, 2) & \dots & \vdots \\ \vdots & \vdots & \vdots & \vdots \\ S_i(M, 1) & S_i(M, 2) & \dots & S_i(M, N) \end{bmatrix}, \quad (3)$$

with

$$S_i(m, l) = \frac{1}{\sqrt{M}} \sum_{k=1}^M X_i(k, l) e^{j2\pi(m-1)(k-1)/M}. \quad (4)$$

Hence, we can obtain the transmitted data matrices of all antennas  $\bar{\mathbf{S}} \in \mathbb{C}^{MN_t \times N}$ , which is given by

$$\bar{\mathbf{S}} = \begin{bmatrix} \mathbf{S}_1 \\ \mathbf{S}_2 \\ \vdots \\ \mathbf{S}_{N_t} \end{bmatrix}. \quad (5)$$

It is worth mentioning that, the cyclic prefix (CP) is added to the transmitted signal  $\bar{\mathbf{S}}$  to transmit. After the transmitted signal undergoes the wireless channel, the signal can be obtained at the receiver.

In the receiver of MIMO-OTFS, we assume that the system has perfect synchronization and channel state information (CSI). After undergoing the time-variant channel with length  $L$  and removing the CP, the received signal  $\mathbf{r}_j^n = [r_j(1, n), r_j(2, n), \dots, r_j(M, n)]^T$  of the  $j$ -th receive antenna on the  $n$ -th frame can be given by

$$\mathbf{r}_j^n = \sum_{i=1}^{N_t} \mathbf{H}_{j,i}^n \mathbf{s}_i^n + \mathbf{z}_j^n, \quad (6)$$

where  $\mathbf{s}_i^n = [S_i(1, n), S_i(2, n), \dots, S_i(M, n)]^T$ , and  $\mathbf{H}_{j,i}^n$  denotes the channel matrix formed by channel time-domain impulse response from the  $i$ -th transmit antenna to the  $j$ -th receive antenna on the  $n$ -th slot, which can be expressed as  $\mathbf{H}_{j,i}^n = \text{circ}[h_1, h_2, \dots, h_L, 0, \dots, 0] \in \mathbb{C}^{M \times M}$ . Moreover,  $\mathbf{z}_j^n$  denotes the noise vector, whose elements obey  $\mathcal{CN}(0, \sigma^2)$ .

According to (6), it is easy to find that the multiple-input multiple-output structure introduces the inter-antenna

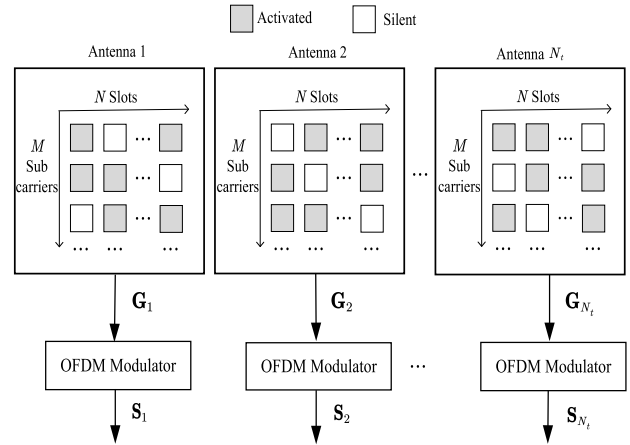


FIGURE 2. The example of the GSM-OFDM systems.

interference (IAI), and hence the demodulation performance suffers from a performance penalty, even though the synchronization and CSI are perfectly obtained at the receiver. More specifically, since each antenna independently transmits the signal  $s_i$ , the receiver needs to determine all signals from the transmit antennas, which imposes the antenna interference. However, to the best of the authors' knowledge, generalized spatial modulation (GSM) plays an important role in reducing the IAI problem at the cost of a moderately decreasing transmission rate. Hence, we will introduce the system structure of GSM-OFDM in the next subsection, to elaborate on the advantage of GSM.

### B. GSM-OFDM

As a promising transmission scheme, GSM-OFDM combines the advantages of SM-OFDM and MIMO-OFDM, achieving a balanced trade-off between the high spectral efficiency and low IAI [20]. More specifically, we assume that the GSM-OFDM system consists of  $N_t$  transmit antennas,  $N_r$  receive antennas,  $M$  subcarriers and  $N$  slots, as portrayed in Fig. 2. Based on the peculiar structure of GSM, each subcarrier is only activated in  $N_s$  selected antennas, to alleviate the IAI problem. This implies that the bit information in GSM-OFDM is carried by the indexes of activated antenna combination, as well as the data symbols in these activated antennas.

To be more explicit, for the  $m$ -th subcarrier and the  $n$ -th slot in GSM-OFDM, a block of  $\lceil \log_2 C_{N_t}^{N_s} \rceil + N_s \log_2 Q$  bits are first divided into two blocks containing  $\lceil \log_2 C_{N_t}^{N_s} \rceil$  and  $N_s \log_2 Q$  bits respectively, where  $Q$  represents the modulation order. Next, the first block of  $\lceil \log_2 C_{N_t}^{N_s} \rceil$  bits is assigned to select the index of the activated antenna combination  $g$  ( $g \in [1, G]$ ), with  $G = 2^{\lceil \log_2(C_{N_t}^{N_s}) \rceil}$ . Then, the remaining block containing  $N_s \log_2 Q$  bits is mapped into  $N_s$   $Q$ -ary quadrature amplitude modulation (QAM) or phase shift keying (PSK) symbols. Finally, these  $Q$ -ary QAM/PSK symbols are transmitted by the activated antennas respectively, which

can be formulated as

$$\mathbf{g}_{m,n} = \begin{bmatrix} 0, \dots, d_{k_1}^{(m,n)}, \dots, d_{k_{N_s}}^{(m,n)}, \dots, 0 \end{bmatrix} \in \mathbb{C}^{1 \times N_t}, \quad (7)$$

$\uparrow$   $k_1^{th}$                        $\uparrow$   $k_{N_s}^{th}$

where  $\{k_1, \dots, k_{N_s}\}$  denotes the indexes of the  $N_s$  activated transmit antennas in the  $g$ -th activated antenna combination, and  $d_k(m, n)$  indicates the  $Q$ -ary QAM/PSK symbol of the  $m$ -th subcarrier and the  $n$ -th slot transmitted by the  $k$ -th antenna, where  $k \in \{k_1, \dots, k_{N_s}\}$ . We note that owing to the special mapping rule, the vector  $\mathbf{g}_{m,n}$  only has  $N_s$  non-zero values, which is capable of mitigating the IAI and reducing the complexity of the receiver.

For simplicity, we rearrange the GSM transmit symbols  $\mathbf{g}_{m,n}$  by all the subcarriers and slots, to obtain the time-frequency domain symbols  $\mathbf{G}_i$  in the  $i$ -th transmit antenna, which can be formulated as

$$\mathbf{G}_i = \begin{bmatrix} \mathbf{g}_{1,1}(i) & \mathbf{g}_{1,2}(i) & \dots & \mathbf{g}_{1,N}(i) \\ \mathbf{g}_{2,1}(i) & \mathbf{g}_{2,2}(i) & \dots & \vdots \\ \vdots & \vdots & \vdots & \vdots \\ \mathbf{g}_{M,1}(i) & \mathbf{g}_{M,2}(i) & \dots & \mathbf{g}_{M,N}(i) \end{bmatrix}, \quad (8)$$

where  $i = 1, 2, \dots, N_t$ , and  $\mathbf{g}_{m,n}(i)$  represents the  $i$ -th element of  $\mathbf{g}_{m,n}$ , with  $m = 1, 2, \dots, M$ ,  $n = 1, 2, \dots, N$ . Similar to (3) and (4), the time-frequency domain symbols  $\mathbf{G}_i$  are then converted to the time-domain symbol  $\mathbf{S}_i$  by the IDFT operation as follows

$$\mathbf{S}_i = \begin{bmatrix} S_i(1, 1) & S_i(1, 2) & \dots & S_i(1, N) \\ S_i(2, 1) & S_i(2, 2) & \dots & \vdots \\ \vdots & \vdots & \vdots & \vdots \\ S_i(M, 1) & S_i(M, 2) & \dots & S_i(M, N) \end{bmatrix}, \quad (9)$$

with

$$S_i(p, n) = \frac{1}{\sqrt{M}} \sum_{m=1}^M \mathbf{g}_{m,n}(i) e^{j2\pi(p-1)(m-1)/M}, \quad (10)$$

where  $p = 1, 2, \dots, M$ . Consequently, the transmitted signals of all antennas  $\mathbf{S}$  can be obtained as  $\mathbf{S} = [\mathbf{S}_1, \mathbf{S}_2, \dots, \mathbf{S}_{N_t}]^T$ , and the received signal can be further calculated by (6), as we derived in the previous subsection.

### C. PROPOSED GSM-OTFS

Inspired by the advantages of GSM in mitigating the IAI, we conceive the generalized spatial modulation and orthogonal time frequency space (GSM-OTFS) scheme, where the special mapping regime of GSM is applied to the Doppler-delay domain, to further improve the performance of the receiver. The details of the proposed scheme are shown as follows.

At the transmitter, we consider a GSM-OTFS system equipped with  $N_t$  transmit and  $N_r$  receive antennas, in which  $N_s$  antennas are selected for data transmission in each subcarrier and time slot. Similarly, in the context of the Doppler-delay domain, we need  $b = N_s \log_2(Q) + \log_2 G$  bits to modulate the GSM transmit symbols, where  $N_s \log_2(Q)$  and  $\log_2 G$  bits are utilized to modulate  $N_s$  constellation symbols and select the index of the activated antenna combination, respectively. Let the  $Q$ -ary QAM/PSK symbol of the  $m$ -th subcarrier and the  $n$ -th slot transmitted by the  $k$ -th antenna be denoted by  $d_k(m, n)$ , where  $m = 1, 2, \dots, M$ ,  $n = 1, 2, \dots, N$ , then the GSM transmit symbols  $\mathbf{t}_{m,n} \in \mathbb{C}^{N_t \times 1}$  can be expressed as

$$\mathbf{t}_{m,n} = \begin{bmatrix} 0, \dots, d_{k_1}^{(m,n)}, \dots, d_{k_{N_s}}^{(m,n)}, \dots, 0 \end{bmatrix}^T, \quad (11)$$

$\uparrow$   $k_1^{th}$                        $\uparrow$   $k_{N_s}^{th}$

where  $\{k_1, \dots, k_{N_s}\}$  indicates the corresponding indexes of the  $N_s$  activated transmit antennas in the selected transmit antenna combination. It is worth mentioning that, although the basic forms of (7) and (11) are similar, the GSM modulations in (7) and (11) are applied to the time-frequency domain and the Doppler-delay domain, respectively. Then, let us denote the  $i$ -th element of the GSM transmit symbols  $\mathbf{t}_{m,n}$  by  $\mathbf{t}_{m,n}(i)$ , we can obtain the Doppler-delay domain symbols  $\mathbf{T}_i$  in the  $i$ -th transmit antenna as follows

$$\mathbf{T}_i = \begin{bmatrix} \mathbf{t}_{1,1}(i) & \mathbf{t}_{1,2}(i) & \dots & \mathbf{t}_{1,N}(i) \\ \mathbf{t}_{2,1}(i) & \mathbf{t}_{2,2}(i) & \dots & \vdots \\ \vdots & \vdots & \vdots & \vdots \\ \mathbf{t}_{M,1}(i) & \mathbf{t}_{M,2}(i) & \dots & \mathbf{t}_{M,N}(i) \end{bmatrix}, \quad (12)$$

where  $i = 1, 2, \dots, N_t$ . For the sake of obtaining the time-frequency domain symbols, the ISFFT operations are then applied to the Doppler-delay domain symbols, resulting in

$$\mathbf{X}_i = \begin{bmatrix} X_i(1, 1) & X_i(1, 2) & \dots & X_i(1, N) \\ X_i(2, 1) & X_i(2, 2) & \dots & \vdots \\ \vdots & \vdots & \vdots & \vdots \\ X_i(M, 1) & X_i(M, 2) & \dots & X_i(M, N) \end{bmatrix}, \quad (13)$$

with

$$X_i(k, l) = \frac{1}{\sqrt{MN}} \sum_{m,n} \mathbf{t}_{m,n}(i) e^{j2\pi\left(\frac{(n-1)(k-1)}{N} - \frac{(m-1)(l-1)}{M}\right)}, \quad (14)$$

where  $k = 1, 2, \dots, M$ ,  $l = 1, 2, \dots, N$ . Note that the ISFFT operation is equivalent to adopt an  $M$ -point DFT and  $N$ -point IDFT in the columns and rows of the matrix  $\mathbf{T}_i$ , and hence, Eqs. (13) and (14) can be rewritten as

$$\mathbf{X}_i = \mathbf{F}_M \mathbf{T}_i \mathbf{F}_N^H, \quad (15)$$

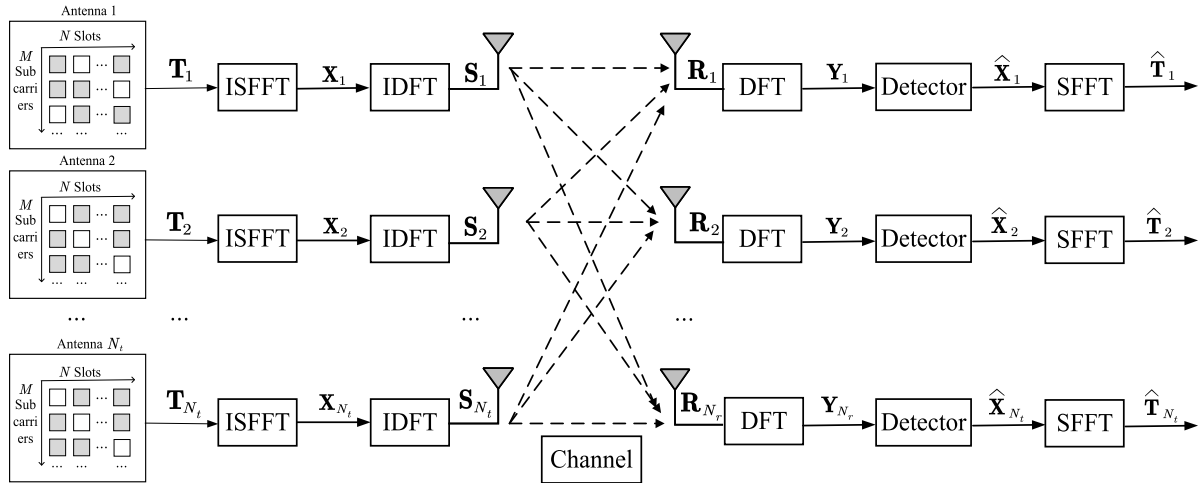


FIGURE 3. The example of the GSM-OTFS systems.

where  $\mathbf{F}_w$  represents the  $w$ -point DFT matrix, with  $w \in \{M, N\}$ . Moreover, the  $w$ -point DFT matrix is assumed to be normalized, namely,  $\mathbf{F}_w^H \mathbf{F}_w = \mathbf{I}_w$ . Hence, the transmitted time domain signals  $\mathbf{S}_i$  of the  $i$ -th antennas that generated by applying an  $M$ -point IDFT to the columns of the matrix  $\mathbf{X}_i$ , can be expressed as

$$\mathbf{S}_i = \mathbf{F}_M^H \mathbf{X}_i = \mathbf{F}_M^H \mathbf{F}_M \mathbf{T}_i \mathbf{F}_N^H = \mathbf{T}_i \mathbf{F}_N^H, \quad (16)$$

where  $\mathbf{S}_i \in \mathbb{C}^{M \times N}$ . After adding the CP to the transmit signal  $\mathbf{S}_i$ , the signal undergoes the channel and then arrives the receiver. In the following analysis, we will discuss two types of channels, i.e., the time dispersive channel and the doubly dispersive channel, and give the corresponding detector of these two channels.

### 1) THE TIME DISPERSIVE CHANNEL

As we mentioned before, in the context of the  $n$ -th slot, the time-domain impulse response of the time dispersive channel

between the  $i$ -th transmit antenna and the  $j$ -th receive antenna can be formulated as  $\mathbf{H}_{j,i}^n = \text{circ}[h_1, h_2, \dots, h_L, 0, \dots, 0] \in \mathbb{C}^{M \times M}$ , which is a circulant matrix. Then, let the transmitted time domain signals of the  $i$ -th antennas in the  $n$ -th time slot be denoted by  $\mathbf{s}_i^n = [S_i(1, n), S_i(2, n), \dots, S_i(M, n)]^T$ , the received signal  $\mathbf{r}_j^n$  of the  $j$ -th receive antenna can be expressed as

$$\mathbf{r}_j^n = \sum_{i=1}^{N_t} \mathbf{H}_{j,i}^n \mathbf{s}_i^n + \mathbf{z}_j^n, \quad (17)$$

which is similar to (6). Furthermore, with the aid of DFT, the circulant channel matrix  $\mathbf{H}_{j,i}^n$  can be diagonalized as

$$\mathbf{H}_{j,i}^n = \mathbf{F}_M^H \mathbf{Q}_{j,i}^n \mathbf{F}_M, \quad (18)$$

where  $\mathbf{Q}_{j,i}^n = \text{diag}[\mathbf{Q}_{j,i}^n(1), \mathbf{Q}_{j,i}^n(2), \dots, \mathbf{Q}_{j,i}^n(M)]$  is the channel main diagonal matrix [24], [25]. Hence, the received

$$\underbrace{\begin{bmatrix} \mathbf{y}_1^n(m) \\ \mathbf{y}_2^n(m) \\ \vdots \\ \mathbf{y}_{N_r}^n(m) \end{bmatrix}}_{\mathbf{y}_{m,n}} = \underbrace{\begin{bmatrix} \mathbf{Q}_{1,1}^n(m) & \mathbf{Q}_{1,2}^n(m) & \cdots & \mathbf{Q}_{1,N_t}^n(m) \\ \mathbf{Q}_{2,1}^n(m) & \mathbf{Q}_{2,2}^n(m) & \cdots & \vdots \\ \vdots & \vdots & \ddots & \vdots \\ \mathbf{Q}_{N_r,1}^n(m) & \mathbf{Q}_{N_r,2}^n(m) & \cdots & \mathbf{Q}_{N_r,N_t}^n(m) \end{bmatrix}}_{\mathbf{Q}_{m,n}} \underbrace{\begin{bmatrix} \mathbf{x}_1^n(m) \\ \mathbf{x}_2^n(m) \\ \vdots \\ \mathbf{x}_{N_t}^n(m) \end{bmatrix}}_{\mathbf{x}_{m,n}} + \underbrace{\begin{bmatrix} \mathbf{w}_1^n(m) \\ \mathbf{w}_2^n(m) \\ \vdots \\ \mathbf{w}_{N_t}^n(m) \end{bmatrix}}_{\mathbf{w}_{m,n}}. \quad (21)$$

$$\underbrace{\begin{bmatrix} \tilde{\mathbf{y}}_1^n \\ \tilde{\mathbf{y}}_2^n \\ \vdots \\ \tilde{\mathbf{y}}_{N_r}^n \end{bmatrix}}_{\tilde{\mathbf{y}}_n} = \underbrace{\begin{bmatrix} \mathbf{V}_{1,1}^n & \mathbf{V}_{1,2}^n & \cdots & \mathbf{V}_{1,N_t}^n \\ \mathbf{V}_{2,1}^n & \mathbf{V}_{2,2}^n & \cdots & \vdots \\ \vdots & \vdots & \ddots & \vdots \\ \mathbf{V}_{N_r,1}^n & \mathbf{V}_{N_r,2}^n & \cdots & \mathbf{V}_{N_r,N_t}^n \end{bmatrix}}_{\mathbf{V}_n} \underbrace{\begin{bmatrix} \mathbf{x}_1^n \\ \mathbf{x}_2^n \\ \vdots \\ \mathbf{x}_{N_t}^n \end{bmatrix}}_{\mathbf{x}_n} + \underbrace{\begin{bmatrix} \mathbf{w}_1^n \\ \mathbf{w}_2^n \\ \vdots \\ \mathbf{w}_{N_t}^n \end{bmatrix}}_{\mathbf{w}_n}. \quad (28)$$



signal  $\mathbf{r}_j^n$  can be detailed as

$$\mathbf{r}_j^n = \sum_{i=1}^{N_t} \mathbf{F}_M^H \mathbf{Q}_{j,i}^n \mathbf{F}_M \mathbf{s}_i^n + \mathbf{z}_j^n. \quad (19)$$

Upon multiplying both sides of (19) by  $\mathbf{F}_M$ , we can obtain the time-frequency domain received signal  $\mathbf{y}_j^n = \mathbf{F}_M \mathbf{r}_j^n$  as follows

$$\begin{aligned} \mathbf{y}_j^n &= \sum_{i=1}^{N_t} \mathbf{F}_M \mathbf{F}_M^H \mathbf{Q}_{j,i}^n \mathbf{F}_M \mathbf{s}_i^n + \mathbf{F}_M \mathbf{z}_j^n \\ &= \sum_{i=1}^{N_t} \mathbf{Q}_{j,i}^n \mathbf{F}_M \mathbf{s}_i^n + \mathbf{w}_j^n \\ &= \mathbf{Q}_{j,1}^n \mathbf{x}_1^n + \mathbf{Q}_{j,2}^n \mathbf{x}_2^n + \dots + \mathbf{Q}_{j,N_t}^n \mathbf{x}_{N_t}^n + \mathbf{w}_j^n, \end{aligned} \quad (20)$$

where  $\mathbf{w}_j^n = \mathbf{F}_M \mathbf{z}_j^n$ ,  $\mathbf{x}_i^n = [X_i(1, n), \dots, X_i(M, n)]^T = \mathbf{F}_M \mathbf{s}_i^n$ . Due to the diagonal property of  $\mathbf{Q}_{j,i}^n$ , Eq. (20) can be rewritten as (21), shown at the bottom of the previous page.

Finally, the estimation of  $\mathbf{x}_{m,n}$  can be readily derived following the zero-forcing (ZF) criterion, which can be expressed as

$$\hat{\mathbf{x}}_{m,n} = \mathbf{Q}_{m,n}^{-1} \mathbf{y}_{m,n}. \quad (22)$$

Moreover, the estimation of  $\mathbf{x}_{m,n}$  based on the minimum mean square error (MMSE) criterion can be given by

$$\hat{\mathbf{x}}_{m,n} = \left( \frac{N_s}{N_t} \mathbf{Q}_{m,n} \mathbf{Q}_{m,n}^H + \sigma^2 \mathbf{I}_{N_r} \right)^{-1} \frac{N_s}{N_t} \mathbf{Q}_{m,n}^H \mathbf{y}_{m,n}. \quad (23)$$

Finally, the delay-Doppler domain received symbols  $\hat{\mathbf{T}}_i$  can be obtained by employing the symplectic finite Fourier transform (SFFT) to the time-frequency domain symbols, which can be expressed as

$$\hat{\mathbf{T}}_i = \mathbf{F}_M^H \hat{\mathbf{X}}_i \mathbf{F}_N. \quad (24)$$

## 2) THE DOUBLY DISPERSIVE CHANNEL

Owing to the extraction of the full channel diversity, the OTFS system is preferable to combat the high Doppler spread in the doubly dispersive channel. We note however that the doubly dispersive channel is unable to be diagonalized, and hence (17)-(19) should be re-derived to satisfy the channel characteristic. More specifically, in the context of  $n$ -th slot, let the time-domain impulse response matrix of the doubly dispersive channel between the  $i$ -th transmit antenna and the  $j$ -th receive antenna be denoted by  $\mathbf{U}_{j,i}^n \in \mathbb{C}^{M \times M}$ , and the element  $U_{j,i}^n(a, b)$  of  $\mathbf{U}_{j,i}^n$  can be detailed as

$$U_{j,i}^n(a, b) = \begin{cases} h(a, a-b), & a-b \in \{0, \dots, L-1\} \\ 0, & \text{otherwise,} \end{cases} \quad (25)$$

where  $a, b \in \{1, 2, \dots, M\}$ . Moreover,  $h(a, a-b)$  denotes the corresponding doubly dispersive channel impulse at  $a$ -th time interval with delay  $a-b$ , where  $L$  represents the maximum delay spread of the channel [26], [27]. Similar to (17), the received signal  $\tilde{\mathbf{r}}_j^n$  of the  $j$ -th receive antenna can be given by

$$\tilde{\mathbf{r}}_j^n = \sum_{i=1}^{N_t} \mathbf{U}_{j,i}^n \mathbf{s}_i^n + \mathbf{z}_j^n. \quad (26)$$

Then, we still apply the DFT operation to the time-domain received signal  $\tilde{\mathbf{r}}_j^n$ , to obtain the time-frequency domain received signal  $\tilde{\mathbf{y}}_j^n = \mathbf{F}_M \tilde{\mathbf{r}}_j^n \in \mathbb{C}^{M \times 1}$  as follows

$$\begin{aligned} \tilde{\mathbf{y}}_j^n &= \sum_{i=1}^{N_t} \mathbf{F}_M \mathbf{U}_{j,i}^n \mathbf{s}_i^n + \mathbf{F}_M \mathbf{z}_j^n \\ &= \sum_{i=1}^{N_t} \mathbf{F}_M \mathbf{U}_{j,i}^n \mathbf{F}_M^H \mathbf{x}_i^n + \mathbf{w}_j^n \\ &= \sum_{i=1}^{N_t} \mathbf{V}_{j,i}^n \mathbf{x}_i^n + \mathbf{w}_j^n, \end{aligned} \quad (27)$$

where  $\mathbf{V}_{j,i}^n = \mathbf{F}_M \mathbf{U}_{j,i}^n \mathbf{F}_M^H$  is the frequency-domain impulse response matrix with quasi-diagonal property, which is different from  $\mathbf{Q}_{j,i}^n$ . Furthermore, Eq. (27) can be rewritten as (28), shown at the bottom of the previous page. where  $\tilde{\mathbf{y}}_n, \mathbf{w}_n \in \mathbb{C}^{N_r M \times 1}$ ,  $\mathbf{V}_n \in \mathbb{C}^{N_r M \times N_r M}$ ,  $\mathbf{x}_n \in \mathbb{C}^{N_t M \times 1}$ . Hence, the OFDM symbols of all transmit antennas in the  $n$ -th slot can be estimated by

$$\hat{\mathbf{x}}_{n,ZF} = \mathbf{V}_n^{-1} \tilde{\mathbf{y}}_n, \quad (29)$$

$$\hat{\mathbf{x}}_{n,MMSE} = \left( \frac{N_s}{N_t} \mathbf{V}_n \mathbf{V}_n^H + \sigma^2 \mathbf{I}_{N_r M} \right)^{-1} \frac{N_s}{N_t} \mathbf{V}_n^H \tilde{\mathbf{y}}_n, \quad (30)$$

which are based on the ZF and MMSE criteria, respectively.

Finally, the output  $\hat{\mathbf{x}}_{n,ZF}$  or  $\hat{\mathbf{x}}_{n,MMSE}$  is transformed to the delay-Doppler domain by SFFT, then the delay-Doppler domain symbols are demodulated to information bits by the hard decision operation.

## III. PROPOSED GAMP DETECTOR FOR GSM-OTFS

In this section, to achieve better detection performance than the MMSE detector, we develop an iterative detector based on the GAMP criterion [23]. Specifically, based on (21), the GSM-OTFS system is modeled as three types of nodes according to the GAMP criterion: (i)  $N_r$  observation nodes corresponding to  $\mathbf{y}_{m,n}$ ; (ii)  $N_r$  variable nodes corresponding to  $\mathbf{d}_{m,n}$ , which denote the reconstructed non-interference vector. (iii)  $N_t$  variable nodes corresponding to  $\mathbf{x}_{m,n}$ ; The GAMP detector iteratively exchanges messages among  $\mathbf{y}_{m,n}$ ,  $\mathbf{d}_{m,n}$  and  $\mathbf{x}_{m,n}$ , which is described in Fig. 4. The various messages passed on this graph include: (a) the prior probability  $P[\mathbf{t}_{m,n} = \beta_i]$  in the  $m$ -th subcarrier and  $n$ -th frame: from the observation node  $\mathbf{y}_{m,n}$  to the variable node  $\mathbf{x}_{m,n}$ ; (b) the mean  $E\{\mathbf{t}_{m,n}\}$  and variance  $Var\{\mathbf{t}_{m,n}\}$  of  $\mathbf{t}_{m,n}$ : from the variable node  $\mathbf{x}_{m,n}$  to the observation node  $\mathbf{y}_{m,n}$ ; (c) the mean  $E\{\mathbf{t}_{m,n}\}$  and variance  $Var\{\mathbf{t}_{m,n}\}$ : from the variable node  $\mathbf{x}_{m,n}$  to the variable node  $\mathbf{d}_{m,n}$ ; (d) the interference symbols  $\mathbf{f}_{m,n}$  in the time-frequency domain: from the variable node  $\mathbf{d}_{m,n}$  to the observation node  $\mathbf{y}_{m,n}$ ;

The details of the GAMP detector are given as follows.

**Step 1:** The mean  $E\{\mathbf{t}_{m,n}\}$  and variance  $Var\{\mathbf{t}_{m,n}\}$  of  $\mathbf{t}_{m,n}$  are calculated by the prior probability  $P[\mathbf{t}_{m,n} = \beta_i]$  as

$$E\{\mathbf{t}_{m,n}\} = \sum_{\beta_i \in \mathbb{S}} \beta_i P[\mathbf{t}_{m,n} = \beta_i], \quad (31)$$

$$\begin{aligned} Var\{\mathbf{t}_{m,n}\} &= \sum_{\beta_i \in \mathbb{S}} \beta_i \beta_i^H P[\mathbf{t}_{m,n} = \beta_i] \\ &\quad - E\{\mathbf{t}_{m,n}\} E\{\mathbf{t}_{m,n}\}^H, \end{aligned} \quad (32)$$

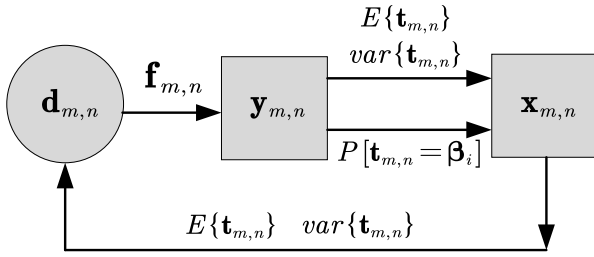


FIGURE 4. Factor graph and messages passing in the proposed GAMP detector.

where  $\mathbb{S}$  denotes the set of all the possible GSM symbols, whose size is  $2^b$ , where  $b = N_s \log_2(Q) + \log_2 G$ . Moreover, the initialization of  $P[t_{m,n} = \beta_i]$  can be expressed as

$$P[t_{m,n} = \beta_i] = \frac{1}{2^b}. \quad (33)$$

Then, the mean symbol  $E\{x_{m,n}\}$  in the time-frequency domain can be obtained by applying the ISFFT operation to  $E\{t_{m,n}\}$ , which is similar to the operation (11)-(14) in Section II.

**Step 2:** Then, the interference symbol  $f_{m,n} \in \mathbb{C}^{N_r \times 1}$  in the time-frequency domain can be reconstructed as

$$f_{m,n} = Q_{m,n} E\{x_{m,n}\} - A_{m,n} d_{m,n}, \quad (34)$$

where  $d_{m,n}$  denotes the no-interference symbol in the time-frequency domain, which can be initialized as  $d_{m,n} = \mathbf{0}_{N_r \times 1}$ . Moreover,  $A_{m,n} \in \mathbb{C}^{N_r \times N_r}$  denotes the power gain matrix which is produced by employing the channel matrix  $Q_{m,n}$  to the symbol  $E\{x_{m,n}\}$ , namely,

$$A_{m,n} = Q_{m,n} M_n Q_{m,n}^H, \quad (35)$$

where  $M_n$  denotes the mean of all the  $M$  subcarriers variance  $Var\{t_{m,n}\}$  of  $t_{m,n}$  on the  $n$ -th frame, which can be calculated by (36), as shown at the bottom of the next page, where  $Var\{t_{m,n}\}_{(i,i)}$  denotes the  $(i, i)$ -th element of  $Var\{t_{m,n}\}$  in (32),  $i \in \{1, 2, \dots, N_t\}$ .

**Step 3:** Update the no-interference symbols  $d_{m,n}$  in the time-frequency domain as

$$d_{m,n} = U_{m,n} (y_{m,n} - f_{m,n}), \quad (37)$$

where  $U_{m,n} \in \mathbb{C}^{N_r \times N_r}$  denotes the power normalized coefficient matrix, which can be expressed as

$$U_{m,n} = (A_{m,n} + \sigma^2 \mathbf{I}_{N_r})^{-1}. \quad (38)$$

**Step 4:** Estimate the mean and variance of the GSM symbol  $t_{m,n}$ . The variances from  $V_{1,n}$  to  $V_{M,n}$ , representing all the sub-carrier symbols  $x_{m,n}$  in the  $n$ -th frame, can be viewed as the same [23] due to the FFT and IFFT operations, which can be expressed as (39), shown at the bottom of the next page. Next, the estimation  $\tilde{x}_{m,n}$  of the OFDM symbol  $x_{m,n}$  can be calculated as

$$\tilde{x}_{m,n} = V_{m,n} Q_{m,n}^H d_{m,n}. \quad (40)$$

Therefore, the final estimation  $\hat{x}_{m,n}$  of  $x_{m,n}$  is expressed as

$$\hat{x}_{m,n} = E\{x_{m,n}\} + \tilde{x}_{m,n}. \quad (41)$$

Furthermore, the delay-Doppler main symbol  $\hat{t}_{m,n}$  can be obtained by employing the SFFT operation to the OFDM symbol  $\hat{x}_{m,n}$ .

On the other hand, similar to the relationship  $Var[w_{m,n}] = \sigma^2 \mathbf{I}_{N_r}$  between the noise matrix  $w_{m,n}$  and the noise value  $\sigma^2$ , the variance value  $\sigma_{(m,n)}^2$  of the variance matrix  $V_{m,n}$  can be denoted as

$$\sigma_{(m,n)}^2 = \frac{\text{trace}\{\text{abs}[V_{m,n}]\}}{N_t}. \quad (42)$$

**Step 5:** The posterior probability  $P[\hat{t}_{m,n} | t_{m,n} = \beta_i]$  can be updated by the mean  $\hat{t}_{m,n}$  and variance  $\sigma_{(m,n)}^2$  as

$$P[\hat{t}_{m,n} | t_{m,n} = \beta_i] = \psi(m, n) e^{-\frac{\|\hat{t}_{m,n} - \beta_i\|^2}{\sigma_{(m,n)}^2}}, \quad (43)$$

where  $\psi(m, n)$  denotes the normalization coefficient.

**Step 6:** Replace the prior probability with posterior probability:  $P[t_{m,n} = \beta_i] = P[\hat{t}_{m,n} | t_{m,n} = \beta_i]$ , then go back for the next iteration, and the number of the max iteration is denoted as  $T$  in the paper.

It is worth noting that the proposed GAMP detector is different from the current detector of [23] in the following two aspects: (a) the detector of [23] is conceived for the single-carrier spatial modulation (SM) systems, which is derived in the time-domain. While, the proposed detector is conceived for the GSM-OTFS system, which is derived in the frequency domain. Specifically, the mean and the variance of the OFDM symbol are calculated based on the mean and the variance of GSM-OTFS transmit symbols  $t_{m,n}$  in (31) and (32) rather than on the mean and the variance of the time-domain symbol. (b) The GSM-OTFS transmitted symbols can be reconstructed by combing three-dimensional information including  $N_r$  antennas,  $M$  subcarriers and  $N$  symbol durations, rather than by only combing  $N_r$  antennas and  $K$  subcarriers in [23]. Specifically, in the detector of [23], the posterior information of the SM symbol  $x_k$  is obtained by the time-domain symbols  $r_k$  in (20) of [23], which is calculated by the IFFT operation of all the  $K$  subcarriers OFDM symbols  $\tilde{r}_k$ , thus it includes the information of  $N_r$  antennas and  $K$  subcarriers. However, in the proposed GAMP detector, the posterior information of the GSM-OTFS symbol is obtained the delay-Doppler domain symbol  $\hat{t}_{m,n}$ , which can be obtained by the SFFT operation of the OFDM symbol  $\hat{x}_{m,n}$  in (41), thus it includes the information of  $N_r$  antennas,  $M$  subcarriers and  $N$  symbol durations.

#### IV. COMPLEXITY ANALYSIS

In this subsection, the complexity of the proposed GAMP detector is given in terms of real flops [28], one flop means a real-valued multiplication or addition. The complexity of the proposed GAMP detector is given in (44), as shown at the bottom of the next page.

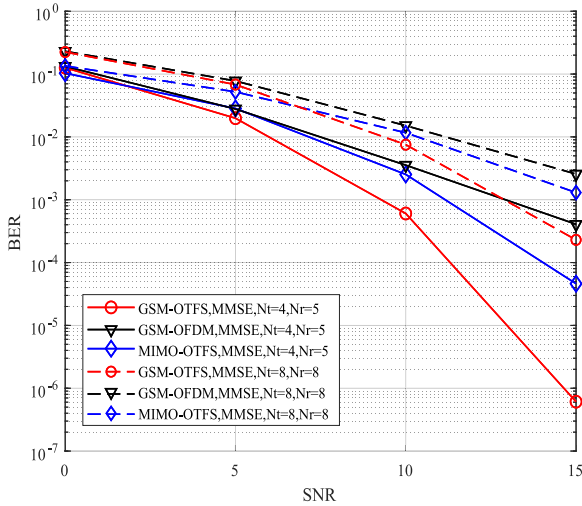


**FIGURE 5.** BER comparison of the MMSE detector for GSM-OTFS, MIMO-OTFS, GSM-OFDM systems with  $N_t = 4$  or  $8$ ,  $N_r = 5$  or  $8$ ,  $M = 256$ ,  $N = 8$  and EVA channel with  $f_d = 0$  Hz.

In fact, the complexity of the proposed GAMP detector is mainly invoked by (31)-(43). More concretely, the number of flops in (31) is given as follows. Specifically,  $E\{\mathbf{t}_{m,n}\}$  needs  $4N_t2^b - 2N_t$  flops and this operation has computed  $MN$  times. So the number of flops for calculating  $E\{\mathbf{t}_{m,n}\}$  is  $(4N_t2^b - 2N_t)MN$  flops. The number of flops for other equations is computed in the similar way.

### V. SIMULATION RESULTS

In this section, we will give a full comparison in terms of bit error rate (BER) performance under the assumption of

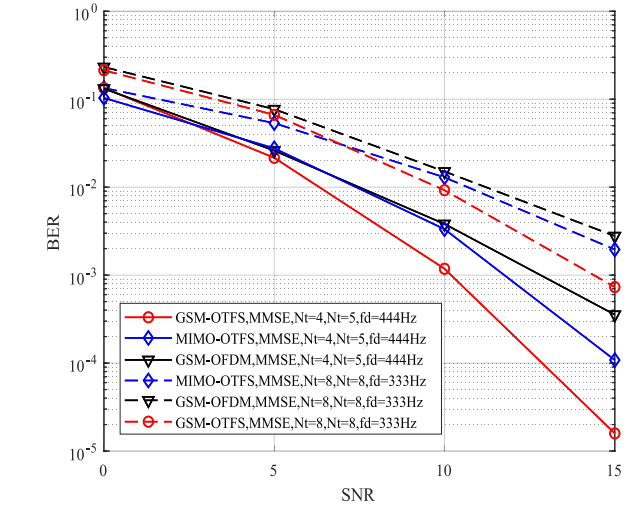


**FIGURE 6.** BER comparison of the MMSE detector for GSM-OTFS, MIMO-OTFS, GSM-OFDM systems with  $N_t = 4$  or  $8$ ,  $N_r = 5$  or  $8$ ,  $M = 64$ ,  $N = 8$  and EVA channel with  $f_d = 444$ Hz or  $333$ Hz.

ideal channel state information at the receiver. Specifically, we simulate the performance of the proposed GSM-OTFS system in the context of the time dispersive channel and the doubly dispersive channel, compared to the traditional GSM-OFDM, MIMO-OTFS systems. What's more, in order to highlight the advantage of the proposed GAMP detector, we compare the equalized performance to that of the MMSE detector, followed by the computational complexity comparison. The details of the system parameter configurations and

$$\mathbf{M}_n = \frac{1}{M} \sum_{m=1}^M \text{diag} \left( \text{Var}\{\mathbf{t}_{m,n}\}_{(1,1)}, \text{Var}\{\mathbf{t}_{m,n}\}_{(2,2)}, \dots, \text{Var}\{\mathbf{t}_{m,n}\}_{(N_t, N_t)} \right), \quad (36)$$

$$\mathbf{V}_{1,n} = \mathbf{V}_{2,n} = \dots = \mathbf{V}_{M,n} = M \left( \sum_{m=1}^M \mathbf{Q}_{m,n}^H \mathbf{U}_{m,n} \mathbf{Q}_{m,n} \right)^{-1}. \quad (39)$$

$$\begin{aligned} C_{GAMP} = & \underbrace{(4N_t2^b - 2N_t)MN}_{(31)} + \underbrace{(10N_t^22^b + 6N_t^2)MN}_{(32)} + \underbrace{(8M^2N + 8MN^2 - 4MN)N_t}_{(ISFFT)} \\ & + \underbrace{(8N_rN_t + 8N_r^2 - 2N_r)MN}_{(34)} + \underbrace{(14N_rN_t - 2N_r^2)MN}_{(35)} + \underbrace{N_tMN}_{(36)} + \underbrace{8N_r^2MN}_{(37)} + \underbrace{(4N_r^3 + 8N_r^2 + N_r)MN}_{(38)} \\ & + \underbrace{(8N_tN_r^2 - 2N_tN_r + 8N_rN_t^2)MN}_{(39)} + \underbrace{4N_t^3N + 8N_t^2N + (8N_rN_t^2 - 2N_tN_r + 8N_tN_r - 2N_t)MN}_{(40)} \\ & + \underbrace{2N_tMN}_{(41)} + \underbrace{(8M^2N + 8MN^2 - 4MN)N_t}_{(SFFT)} + \underbrace{N_tN}_{(42)} + \underbrace{(6N_t + 3)MN2^b - MN}_{(43)} \end{aligned} \quad (44)$$



TABLE 1. The simulation parameter configurations.

Fig.	Scheme	$N_t$	$N_r$	$N_s$	Modulation method	$M$	$N$	Maximum Doppler frequency shift $f_d$ (Hz)
5	MIMO-OTFS	4, 8	5, 8	/	BPSK	256	8	0
	GSM-OFDM, GSM-OTFS	4, 8	5, 8	1, 2	QPSK	256	8	0
6	MIMO-OTFS	4, 8	5, 8	/	BPSK	64	8	444, 333
	GSM-OFDM, GSM-OTFS	4, 8	5, 8	1, 2	QPSK	64	8	444, 333
7	GSM-OTFS	8	8	2	QPSK	256	8	0
8	GSM-OTFS	8	8	2	QPSK	64	8	333

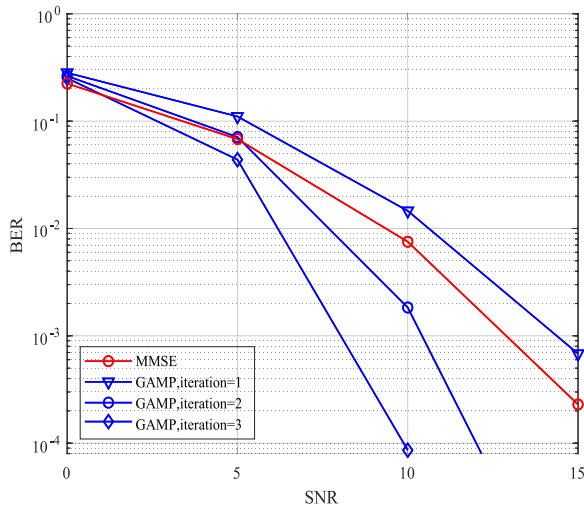


FIGURE 7. BER comparison of MMSE and the proposed GAMP detectors for GSM-OTFS systems with  $N_t = 8$ ,  $N_r = 8$ ,  $M = 256$ ,  $N = 8$  and EVA channel with  $f_d = 0$ Hz.

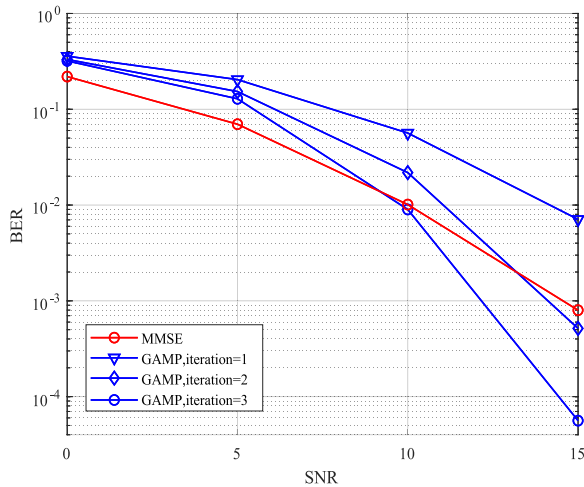


FIGURE 8. BER comparison of MMSE and the proposed GAMP detectors for GSM-OTFS systems with  $N_t = 8$ ,  $N_r = 8$ ,  $M = 64$ ,  $N = 8$  and EVA channel with  $f_d = 333$ Hz.

the Extended Vehicular A (EVA) channel configurations are shown in Table. 1 and 2, respectively.

Fig. 5 portrays the BER performance of the GSM-OFDM, MIMO-OTFS, and the proposed GSM-OTFS systems in the context of the EVA channel with  $f_d = 0$ , based on the MMSE

TABLE 2. The EVA channel configurations.

Delay of each multipath (ns)	(0,30,150,310,370,710,1090,1730,2510)
Average power of each multipath (dB)	(0,-1.5,-1.4,-3.6,-0.6,-9.1,-7.0,-12.0,-16.9)
Subcarrier spacing (kHz)	15
Carrier frequency (GHz)	4

detector in (23). Moreover, these systems have the same spectral efficiency, i.e., 4 (bit/s/Hz) in solid lines and 8 (bit/s/Hz) in dotted lines, respectively. It can be seen from the solid lines in Fig. 5 that the proposed GSM-OTFS system results in a significantly improved BER performance, while keeping the same spectral efficiency. The results of this figure validate our analysis that, the special mapping regime of GSM is capable of mitigating the IAI, and further improving the receiver performance. The above observation can be further augmented with the aid of the dotted lines of Fig. 5, where the number of transmit antennas and receive antennas increases from 4 to 8, 5 to 8, respectively. With the increased IAI, the proposed GSM-OTFS scheme still provides a considerable performance gain compared to that of the traditional GSM-OFDM, MIMO-OTFS, which further indicates that GSM-OTFS is capable of alleviating the IAI.

Furthermore, since the conventional OTFS is proposed for a doubly dispersive channel, we introduce the high Doppler spread into the simulation, for the sake of further investigating the performance of our proposed GSM-OTFS scheme. Fig. 6 compares the BER performance of the GSM-OFDM, MIMO-OTFS, and the proposed GSM-OTFS systems in the context of the EVA channel with  $f_d = 333$ Hz or  $f_d = 444$ Hz, i.e., the vehicle speed is 90 km/h or 120 km/h, respectively. It is worth noting that since the high Doppler spread has been introduced into the simulation, the MMSE detector in (23) is replaced by the MMSE detector in (30). We note in the solid lines of Fig. 6 that, the proposed GSM-OTFS system still achieves the optimal BER performance among all the systems, which approximately exhibits 3 dB performance gain at a BER of  $10^{-3}$ , compared to that of MIMO-OTFS and GSM-OFDM. Moreover, we observe that in the dotted lines of Fig. 6, the proposed GSM-OTFS systems are capable of providing better performance than the conventional MIMO-OTFS and GSM-OFDM, on the condition that extremely high IAI and ICI exist. Hence, the GSM-OTFS scheme is capable of reaping

the advantage in combating the impact of the Doppler shift and alleviating the IAI.

However, another feature observed for Fig. 6 is that the gap between GSM-OTFS and GSM-OFDM is smaller, when the number of transmitted antennas is increased. The reason for this trend is that the MMSE detector under the higher IAI and ICI is not as effective as it is at low IAI and ICI, and the GSM-OTFS scheme further applies the SFFT operation to the inaccurate equalized results, which may lead to less accurate demodulated results. Hence, it is of paramount importance to develop detector that outperform the MMSE detector.

In order to characterize the detected performance of the proposed GAMP detector, we plot the BER comparison of the conventional MMSE and the proposed GAMP detector in Figs. 7 and 8. Fig. 7 portrays the BER performance of these two detectors in the context of  $N_t = 8$ ,  $N_r = 8$ ,  $M = 256$ ,  $N = 8$  and EVA channel with  $f_d = 0\text{Hz}$ . From the results we observe that the GAMP detector can achieve better performance than the conventional MMSE ones, after a finite number of iterations. More specifically, after two iterations, the proposed GAMP detector can attain around 2.5 dB gain at the BER of  $10^{-3}$  compared to MMSE. The reason for this trend is that the GAMP detector is an iterative detector, which is capable of providing a more reliable belief of the channel state information, by fully utilizing the property of the transmitted symbol. These observations indicate the effectiveness of the proposed GAMP detector, in the context of  $f_d = 0\text{Hz}$ .

While in the context of  $f_d = 333\text{Hz}$ , the trend of the proposed GAMP detector is slightly different from Fig. 7. Fig. 8 portrays the BER comparison of the conventional MMSE and proposed GAMP detector, in the context of the doubly dispersive channel with  $f_d = 333\text{Hz}$ , while the number of subcarriers decreased from 256 to 64 compared to Fig. 7. From the results we observe that the GAMP detector entails more iterations to achieve better performance than MMSE, due to the deterioration of the channel state. However, it still provides about 2.5 dB performance gain compared to MMSE at a BER of  $10^{-3}$ , after 3 iterations. Consequently, in the context of the doubly dispersive channel, GAMP may be less effective but still provide a moderate performance gain.

## VI. CONCLUSION

In this paper, the generalized spatial modulation techniques have successfully been applied to OTFS in order to reap their advantages in alleviating the ICI and combating the high Doppler spreads. With a careful design, we exhibit the transceiver architecture of the proposed GSM-OTFS scheme in the context of the time dispersive channel and doubly dispersive channel. Our simulation results demonstrated that the proposed system has the potential to achieve better BER performance compared to conventional MIMO-OTFS and GSM-OFDM systems. Furthermore, an iterative detector based on GAMP has been proposed for the sake of obtaining better performance than the MMSE detector. The simulation results validated the effectiveness of the proposed GAMP detector for providing better BER performance, after finite iterations.

Hence, with the combination of the GAMP detector, GSM-OTFS may be an attractive transmission waveform in the high Doppler spreads scenario.

However, further study is still required in order to illustrate the impact of the different number of activated antennas on BER performance. What's more, we will provide more detailed comparisons between SM-OTFS and GSM-OTFS in spectral efficiency and BER performance in our future work.

## REFERENCES

- [1] X. You, C. Wang, J. Huang, X. Gao, and Z. Zhang, "Towards 6G wireless communication networks: Vision, enabling technologies, and new paradigm shifts," *Sci. China Inf.*, vol. 64, no. 1, pp. 1–74, Nov. 2020.
- [2] B. Farhang-Boroujeny, "OFDM versus filter bank multicarrier," *IEEE Signal Process. Mag.*, vol. 28, no. 3, pp. 92–112, May 2011.
- [3] T. Hwang, C. Yang, G. Wu, S. Li, and G. Y. Li, "OFDM and its wireless applications: A survey," *IEEE Trans. Veh. Technol.*, vol. 58, no. 4, pp. 1673–1694, May 2009.
- [4] T. Dean, M. Chowdhury, and A. Goldsmith, "A new modulation technique for Doppler compensation in frequency-dispersive channels," in *Proc. PIMRC*, 2017, pp. 1–7.
- [5] R. Hadani, S. Rakib, M. Tsatsanis, A. Monk, A. J. Goldsmith, A. F. Molisch, and R. Calderbank, "Orthogonal time frequency space modulation," in *Proc. IEEE Wireless Commun. Netw. Conf. (WCNC)*, Mar. 2017, pp. 1–6.
- [6] R. Hadani and A. Monk. (2017). *OTFS—A Novel Modulation Technique Meeting 5G High Mobility and Massive MIMO Challenges*. [Online]. Available: <https://www.cohere-technologies.com/wpcontent/uploads/2017/10/OTFS-Physics-White-Paper.pdf>
- [7] A. Farhang, A. R. Reyhani, L. E. Doyle, and B. Farhang-Boroujeny, "Low complexity modem structure for OFDM-based orthogonal time frequency space modulation," *IEEE Wireless Commun. Lett.*, vol. 7, no. 3, pp. 344–347, Jun. 2018.
- [8] P. Raviteja, K. T. Phan, Y. Hong, and E. Viterbo, "Interference cancellation and iterative detection for orthogonal time frequency space modulation," *IEEE Trans. Wireless Commun.*, vol. 17, no. 10, pp. 6501–6515, Oct. 2018.
- [9] P. Raviteja, Y. Hong, E. Viterbo, and E. Biglieri, "Practical pulse-shaping waveforms for reduced-cyclic-prefix OTFS," *IEEE Trans. Veh. Technol.*, vol. 68, no. 1, pp. 957–961, Jan. 2019.
- [10] Z. Wei, W. Yuan, S. Li, and J. Yuan, "Orthogonal time-frequency space modulation: A promising next-generation waveform," *IEEE Wireless Commun.*, vol. 28, no. 4, pp. 136–144, Aug. 2021.
- [11] A. Rezazadehrehyani, A. Farhang, M. Ji, R. R. Chen, and B. Farhang-Boroujeny, "Analysis of discrete-time MIMO OFDM-based orthogonal time frequency space modulation," in *Proc. IEEE Int. Conf. Commun. (ICC)*, Kansas City, MO, USA, May 2018, pp. 1–6.
- [12] W. Shen, L. Dai, J. An, P. Fan, and R. W. Heath, Jr., "Channel estimation for orthogonal time frequency space (OTFS) massive MIMO," *IEEE Trans. Signal Process.*, vol. 67, no. 16, pp. 4204–4217, Aug. 2019.
- [13] M. Kollengode Ramachandran and A. Chockalingam, "MIMO-OTFS in high-Doppler fading channels: Signal detection and channel estimation," in *Proc. IEEE Global Commun. Conf. (GLOBECOM)*, Dhabhi, United Arab Emirates, Dec. 2018, pp. 206–212.
- [14] G. D. Surabhi, R. M. Augustine, and A. Chockalingam, "On the diversity of uncoded OTFS modulation in doubly-dispersive channels," *IEEE Trans. Wireless Commun.*, vol. 18, no. 6, pp. 3049–3063, Jun. 2019.
- [15] Y. Yang, Z. Bai, K. Pang, P. Ma, H. Zhang, X. Yang, and D. Yuan, "Design and analysis of spatial modulation based orthogonal time frequency space system," *China Commun.*, vol. 18, no. 8, pp. 209–223, Aug. 2021.
- [16] M. Di Renzo, H. Haas, A. Ghayeb, S. Sugiura, and L. Hanzo, "Spatial modulation for generalized MIMO: Challenges, opportunities, and implementation," *Proc. IEEE*, vol. 102, no. 1, pp. 56–103, Jan. 2014.
- [17] P. Yang, Y. Xiao, Y. Guan, and K. Hari, "Single-carrier SM-MIMO: A promising design for broadband large-scale antenna systems," *IEEE Commun. Surveys Tuts.*, vol. 18, no. 3, pp. 1687–1716, 3rd Quart., 2016.
- [18] P. Yang, M. Di Renzo, and Y. Xiao, "Design guidelines for spatial modulation," *IEEE Commun. Surveys Tuts.*, vol. 17, no. 1, pp. 6–26, 1st Quart., 2014.
- [19] J. Wang, S. Jia, and J. Song, "Generalised spatial modulation system with multiple active transmit antennas and low complexity detection scheme," *IEEE Trans. Wireless Commun.*, vol. 11, no. 4, pp. 1605–1615, Apr. 2012.

[20] B. Gong, L. Gui, S. Luo, Y. L. Guan, Z. Liu, and P. Fan, "Block pilot based channel estimation and high-accuracy signal detection for GSM-OFDM systems on high-speed railways," *IEEE Trans. Veh. Technol.*, vol. 67, no. 12, pp. 11525–11536, Dec. 2018.

[21] S. Rangan, "Generalized approximate message passing for estimation with random linear mixing," in *Proc. IEEE Int. Symp. Inf. Theory*, Saint Petersburg, Russia, Jul. 2011, pp. 2168–2172.

[22] Q. Guo, D. Huang, S. Nordholm, J. Xi, and Y. Yu, "Iterative frequency domain equalization with generalized approximate message passing," *IEEE Signal Process. Lett.*, vol. 20, no. 6, pp. 559–562, Jun. 2013.

[23] Y. Zhao, Y. Xiao, P. Yang, B. Dong, R. Shi, and K. Deng, "Generalized approximate message passing aided frequency domain turbo equalizer for single-carrier spatial modulation," *IEEE Trans. Veh. Technol.*, vol. 67, no. 4, pp. 3630–3634, Apr. 2018.

[24] P. Raviteja, E. Viterbo, and Y. Hong, "OTFS performance on static multipath channels," *IEEE Wireless Commun. Lett.*, vol. 8, no. 3, pp. 745–748, Jun. 2019.

[25] J. Zhang, A. D. S. Jayalath, and Y. Chen, "Asymmetric OFDM systems based on layered FFT structure," *IEEE Signal Process. Lett.*, vol. 14, no. 11, pp. 812–815, Nov. 2007.

[26] C. Jin, Z. Bie, X. Lin, W. Xu, and H. Gao, "A simple two-stage equalizer for OTFS with rectangular Windows," *IEEE Commun. Lett.*, vol. 25, no. 4, pp. 1158–1162, Apr. 2021.

[27] L. Rugini, P. Banelli, and G. Leus, "Simple equalization of time-varying channels for OFDM," *IEEE Commun. Lett.*, vol. 9, no. 7, pp. 619–621, Jul. 2005.

[28] L. Xiao et al., "Efficient compressive sensing detectors for generalized spatial modulation systems," *IEEE Trans. Veh. Technol.*, vol. 66, no. 2, pp. 1284–1298, Feb. 2017.



**HAO CHEN** received the B.E. degree in electronic information engineering from the University of Electronic Science and Technology of China (UESTC), in 2020, where she is currently pursuing the master's degree with the National Key Laboratory of Science and Technology on Communications. Her research interests include the multiple-input multiple-output technologies and space modulation technologies toward future wireless communication systems.



**YUE XIAO** (Member, IEEE) received the Ph.D. degree in communication and information systems from the University of Electronic Science and Technology of China (UESTC), in 2007. He is currently a Professor with the National Key Laboratory of Science and Technology on Communications, UESTC. He has published more than 100 international journals and has been in-charge of more than 20 projects in the area of Chinese 3G/4G/5G wireless communication systems.

He holds more than 50 Chinese and PCT patents on wireless systems. His research interests include system design and signal processing toward future wireless communication systems. He is currently the Associate Editor of *IEEE COMMUNICATIONS LETTERS*.



**TIEBIN WANG** received the Ph.D. degree from Northeast Forestry University, in 2013. He is currently a Lecturer with the Information and Computer Engineering College, Northeast Forestry University. He has been involved with some research projects including forest communications and environment sensing for dog-training with wireless sensor networks. His research interests include mobile communication and multicarrier techniques.



**XUEMEI GUAN** received the Ph.D. degree from Northeast Forestry University, in 2011. She is currently a Teacher with the College of Mechanical and Electrical Engineering, Northeast Forestry University. She has published more than ten international journals and has been in charge of more than ten projects in the area of deep learning and wood dyeing.



**SHIWEN FAN** received the B.S. degree from the University of Electronic Science and Technology of China (UESTC), Chengdu, China, in 2013, where he is currently pursuing the Ph.D. degree with the National Key Laboratory of Science and Technology on Communications. His research interests include wireless communications and communication theory. In particular, he is very interested in signal detection of wireless communication systems.



**WENLONG SONG** received the Ph.D. degree from Northeast Forestry University (NEFU), in 2008. He is currently a Professor with the College of Mechanical and Electrical Engineering, NEFU. He has published more than 30 international journals and has been in charge of more than 20 projects in the area of Chinese automatic systems. His research interests include the plant life information detection technology and detection and control technology of forestry engineering processing process.

...